Clays and Clay Minerals, Vol. 61, No. 5, 424–439, 2013.

PREPARATION AND CHARACTERIZATION OF Fe-, Co-, AND Ni-CONTAINING Mg-Al-LAYERED DOUBLE HYDROXIDES

HILDE CURTIUS[1], GABRIEL KAISER[1], KONSTANTIN ROZOV[1], ANDREAS NEUMANN[1], KATHY DARDENNE[2], AND DIRK BOSBACH[1]

[1] Institute for Energy and Climate Research (Nuclear Waste Management and Reactor Safety, IEK-6), Forschungszentrum Jülich, 52425 Jülich, Germany

[2] Karlsruhe Institute of Technology (KIT), Institute for Nuclear Waste Disposal (INE), Hermann-von-Helmholtz-Platz 1, 76344 Eggenstein-Leopoldshafen, Germany

Abstract—Syntheses of Fe-, Co-, and Ni-containing Mg-Al-layered double hydroxides (LDHs) are described here because Fe, Co, and Ni represent the major constituents in steel containers used for storing spent nuclear fuel. Much evidence exists for the formation of LDHs during the corrosion of such containers under repository-relevant conditions. Because of their anion-exchange properties, LDHs can be considered as materials with the potential to retain and immobilize anionic radionuclides. Evaluation of the thermodynamic properties of LDHs is essential for reliable prediction of their behavior (solubility, anion exchange properties) in geochemical environments. The impact on the thermodynamic properties of the isostructural incorporation of divalent cations into the LDH was the main focus of the present study.

Mg-Al-Cl-LDH and the Fe-, Co-, and Ni-doped LDHs were synthesized by the co-precipitation method and then characterized (using powder X-ray diffraction (PXRD), extended X-ray absorption fine structure (EXAFS), X-ray absorption near edge structure (XANES), Fourier-transform infrared spectroscopy (FTIR), scanning electron microscopy energy-dispersive X-ray spectroscopy (SEM-EDX), and thermogravimetric analyses (TGA)).

The PXRD and EXAFS analyses indicated that all synthesized samples were pure LDHs where Co, Ni, and Fe were incorporated isostructurally. The EXAFS and XANES results demonstrated that Ni and Co were incorporated as divalent cations and Fe as a trivalent cation. Thermodynamic calculations were performed assuming an equilibrium state between aqueous solutions and corresponding precipitates after synthesis. The first estimates of the molar Gibbs free energies for Fe-, Co-, and Ni-containing LDHs at 70ºC were provided. The calculated Gibbs free energy of the pure Mg-Al-LDH (−3629 kJ/mol) was slightly less than those for Fe-, Co-, and Ni-containing compositions (−3612±50, −3604±50, −3593±50kJ/mol).

Key Words— EXAFS, Corrosion Products, Layered Double Hydroxides, Solubility, Thermodynamic Modeling.

INTRODUCTION

Layered double hydroxides (LDHs), or the so-called 'anionic clays,' constitute a class of lamellar compounds containing positively charged brucite-like layers and exchangeable anions in the interlayers (Miyata, 1975). Besides the anions, water is also present in the interlayer spaces. The general formula that represents this kind of material is $[M^{2+}_{1-x}M^{3+}{}_x][A^{n-}_{x/n}\cdot m\mathrm{H_2O}]$, where M^{2+} and M^{3+} are di- and trivalent metal cations, respectively, x is the molar ratio of $M^{3+}/(M^{2+} + M^{3+})$, and A is an interlamellar anion with charge n^-. The structure of these compounds can be visualized as a brucite ($Mg(OH)_2$)-like octahedral layer in which part of the Mg^{2+} is replaced isomorphously with trivalent cations and the positive charge of the layer is balanced by equal negative charge from the interlayer solvated anions (*e.g.* CO_3^{2-}, NO_3^-, Cl^-, *etc.*) (Cavani *et al.*, 1991). A large number of LDHs with variations in the M^{2+}–M^{3+} cation pair including M^+–M^{3+} (*e.g.* Li–Al) and M^{2+}–M^{4+} (*e.g.* Co-Ti) and their applications have been documented (Taylor, 1984).

Layered double hydroxides have been the subject of intensive research because of their wide applications as catalysts and as anion exchangers. In the nuclear field, the interest is in LDHs as anion exchangers because long-lived anionic fission products (*e.g.* ^{129}I, ^{79}Se, ^{99}Tc, *etc.*) are very mobile and scarcely retarded by the multi-barrier system of many disposal sites (NAGRA 02-05). Different waste matrices in contact with groundwater corrode and LDHs form as a corrosion product. When cementitious waste corrodes in salt solutions the so-called "Friedel's salt" is formed (Renaudin *et al.*, 1999). Friedel's salt is an anion-exchange mineral belonging to the class of LDHs with the general formula $Ca_2Al(OH)_6(Cl,OH)\cdot 2H_2O$. In the octahedral layer, Ca rather than Mg is present as the divalent cation. In $MgCl_2$-$CaCl_2$ salt solution, nuclear-waste glass and

* E-mail address of corresponding author:
h.curtius@fz-juelich.de
DOI: 10.1346/CCMN.2013.0610503

basaltic-glass alteration processes occurred and the formation of LDHs was observed (Abdelouas *et al.*, 1994). In many countries, spent fuel will be disposed in canisters made of iron. In contact with groundwater, iron will corrode and hydrogen will be produced, creating a reducing environment. Under these conditions, magnetite and a LDH-like compound known as 'green rust' (Fe(II)- and Fe(III)-containing LDHs) were identified as corrosion products (Cui and Spahiu, 2002).

In Germany, irradiated research-reactor fuel elements with uranium silicide as the fuel will be stored in cast iron containers and, after an interim period of dry storage, direct disposal in deep geological formations is planned. Research-reactor fuel samples (UAl_x-Al- and U_3Si_2-Al-types) were leached in the presence of Fe(II) aqueous species in a repository-relevant $MgCl_2$-rich salt brine. Mg-Al-layered double hydroxides and the 'green rust' were identified as crystalline secondary phase components (Mazeina *et al.*, 2003; Curtius *et al.*, 2009, 2010).

Besides iron as a major component of the spent-fuel container, the elements Ni and Co are present also and, therefore, the possible formation of solid solutions of (Mg,Co)/Al-LDH, (Mg,Ni)/Al, and (Mg,Fe)/Al-LDHs in a final repository cannot be ruled out. Many research groups have focused on these LDHs because they may be useful as catalysts in the selective conversion of acetone to other valuable products such as methyl isobutyl ketone, methyl isobutyl carbinol, and mesityl oxide. These compounds are mostly prepared using the co-precipitation method with carbonate in the interlayer. Note that during the co-precipitation-step, Ni(II) and Co(II) were found to substitute easily for Mg(II) (Unnikrishnan and Narayanan, 1999), whereas Fe present as Fe(III) substituted for the Al(III) ion. Information on the thermodynamic and stability properties of pure and complex solid solutions of LDHs is very sparse. In recent years the first estimates of thermodynamic properties and aqueous solubilities of Mg-Al-LDHs were obtained by applying calorimetric measurements (Allada *et al.*, 2005), and for Mg-Al-Fe(III)-LDH by combining the results of co-precipitation and long-term (>200 days) dissolution experiments (Rozov *et al.*, 2010, 2011).

The present study focused on (1) the synthesis of Co-, Ni-, and Fe-containing Mg-Al-LDHs, (2) their structural properties, and (3) their thermodynamic properties in order to assess the stability and aqueous solubility in comparison to a pure Mg-Al-LDH.

EXPERIMENTAL

Deionized water was boiled and stored under an argon atmosphere before use. The chemicals were of analytical grade and used without further treatment. All experiments and working steps were performed under an argon atmosphere.

Synthesis of LDHs

The Mg-Al-LDH was synthesized using the co-precipitation method at controlled pH conditions as described by Weiss and Toth (1996) with some modifications in relation to the purification and drying steps. A detailed description was given by Curtius and Kattilparampil (2005).

The Co-, Ni-, and Fe-bearing LDHs were prepared according to the same co-precipitation method. Specifically, 250 mL of water was placed in a three-necked glass flask and a pH of 10.0±0.1 was achieved using 2 M NaOH. A mixed aqueous solution containing $MgCl_2{\cdot}6H_2O$ (0.29 moles), $CoCl_2$ (0.01 moles), or $FeCl_2{\cdot}4H_2O$ (0.01 moles); or $NiCl_2{\cdot}6H_2O$ (0.01 moles) and $AlCl_3{\cdot}6H_2O$ (0.1 moles) in 250 mL of water was added over a period of 5 h while the pH was maintained at 10.0±0.1 by simultaneous addition of 2 M NaOH. During the precipitation process the temperature was maintained at 70±1ºC. After the addition was complete, the temperature was raised to 90±1ºC and stirring was continued for 24 h. After cooling to room temperature (25±1ºC), the precipitate formed was filtered and then dialyzed at 60±1ºC for 72 h. For this washing step the dialysis hose was filled with the precipitated solid and then placed in a 2 L vessel containing deionized water. The water was changed three times a day until it was chloride-free (chloride measurements were performed using the cuvette test LCK 311, Dr. Lange^{TM}). The detection limit of the chloride test used was 2.82×10^{-5} moles L^{-1}. Then the precipitate was filtered and dried in a desiccator under argon.

The substances obtained were characterized by photometry (UV-visible spectrometer), PXRD, EDX, EXAFS, TGA, FTIR, and inductively coupled plasma-optical emission spectroscopy (ICP-OES).

Characterization techniques

Scanning electron microscopy (SEM). Investigation by SEM was performed using the environmental scanning electron microscope FEI Quanta 200 F (FEI, Oregon, USA). The measurements were carried out in low-vacuum mode at 0.6 mbar (20 kV, spot size 4, working distance 10 mm). The counting time was 50 s and the energy setting of the energy-dispersive analysis was 20 keV. The resolution was 132.40 eV. When using this mode, sputtering of the samples with gold or carbon was unnecessary and analytical artifacts were, thus, avoided. The samples were prepared as powders on adhesive carbon tabs. The microscope is equipped with the EDX-system Genesis (EDAX).

Photometric/UV-visible analyses. The chloride content in the precipitates and in the corresponding supernatant liquids was determined by photometric measurement (wavelength of 300−600 nm, with a maximum reflection at 468 nm) (Dr. Lange photometer CADAS 100) (Dr.

https://doi.org/10.1346/CCMN.2013.0610503 Published online by Cambridge University Press

Lange, Berlin, Germany) using a test cuvette (LCK 311, Dr. Lange™). Aliquots of the liquid phases were measured, over the wavelength range mentioned above, after dilution (1 to 1000) with water. Each solid (100 mg) was dissolved in 10 mL of a 2 M HNO_3 solution. Then another dilution (1 to 50) with water was performed. This solution was measured using test cuvette LCK 311 (path length = 10 mm).

Determination of the oxidation state of Fe in Mg-Al-Fe-containing LDHs. The presence of Fe(III) in the Fe-bearing LDH was determined by the formation of an Fe(III) thiocyanate complex (Hollemann and Wiberg, 1976) and the photometric measurement was performed using a Dr. Lange Photometer CADAS 100 instrument. In the first step, 200 mg of the Fe-bearing LDH was dissolved in 5 mL of concentrated HNO_3 solution and then diluted with water to a volume of 20 mL. Then 50 µL of this sample solution was added to 50 mL of water. Next, 15 mL of TBP (tributylphosphate) and 15 mL of a NH_4SCN (20 wt.%) solution were added. The mixture was shaken for 10 min. Finally, 5 mL of the organic phase was separated and dried with Na_2SO_4. After 10 min, ~2 mL of this solution was used for the measurement. The concentration of Fe(III) was calculated according to Beer-Lambert Law. The analytical error was in the range of ±5%. Pure $Fe(III)Cl_3$ and $Fe(II)Cl_2$ salt solutions were used as internal standard solutions.

ICP-OES analyses. The Mg, Al, Fe, Co, Ni, and Na contents in the solid and liquid phases were determined by ICP-OES using a Perkin-Elmer ICP-OES instrument (Thermo Fisher Scientific Model 11189 (Massachusetts, USA)). The liquid samples were analyzed directly without dilution steps. Each solid sample (100 mg) was dissolved in 10 mL of a 2 M HNO_3 solution. This solution was further diluted (1 to 100) with a 0.1 M HNO_3 solution and then the measurement was performed.

Thermogravimetric analyses (TGA). The TGA measurements were carried out using a NETSCH STA 449 C Jupiter™ instrument (Netsch, Selb, Germany). In the temperature range between 25 and 1000ºC the heating rate was 10ºC/min. The measurements were carried out under nitrogen flow. Within the measurements the interlayer water contents, hydroxyl groups, and chloride anions were determined. The temperatures of removal of interlayer water, chloride, and hydroxyl groups were also determined.

FTIR analyses. The interlayer composition (anion, interlayer water) was determined by FTIR analysis using a Bruker Equinox™ (Massachusetts, USA) spectrometer with the KBr pellet technique. Approximately 200 mg of KBr and ~2 mg of LDH were mixed carefully and a pressure of 10 tons was applied and held constant for 3 min to prepare each pellet. The IR spectra were recorded in the range 4000 to 400 cm^{-1}.

XRD measurements – Phase identification. The XRD measurements were carried out using a D8 Advance powder diffractometer from Bruker AXS (Karlsruhe, Germany). The structural analysis and the phase quantification were carried out using the *BGMN* software package (Bergmann *et al.*, 1998). The program is based on the fundamental parameter approach (FPA) which considers the diffractometer geometry, *i.e.* physical parameters, in order to describe the device function (Klug and Alexander, 1974).

The goniometer of the diffractometer features a θ-θ Bragg-Brentano geometry with a radius of 250 mm. For the XRD measurements, CuKα radiation at 30 kV and 45 mA was applied. The intensity gained was registered by a 1D VÅntec line detector. A nickel filter was inserted to suppress parasitic CuKβ radiation. An automatic aperture system was used to maintain a constant X-ray irradiation length on the sample of 3 mm. Primary Soller slits with a device angle of 2.376º were also applied to reduce divergence of the incident beam. The XRD measurements were carried out in continuous mode with a step size of 0.028º and with 1 s/step over the range 5 to 85º2θ.

A non-certified Zincite p.A. standard of known weight (10 wt.%) was added as an internal standard for goniometer alignment corrections, using the *DiffracPlus Eva* software (by Bruker-AXS), which references the observed Zincite reflections to entry no. 00-036-1451 of the powder diffraction file PDF-2 database of the International Centre for Diffraction Data (ICDD). The magnitude of these corrections was ~0.1 mm. Zincite was also used (by adding it to the LDH and then applying Rietveld to determine the amounts of phases) to quantify byproducts (crystalline and/or amorphous) which may have formed during the LDH syntheses.

Refinement of real structure parameters of the LDH compounds using the Rietveld method was demonstrated by Ufer *et al.* (2008). Practical considerations of that investigation, which refer to the sample preparation of LDH compounds and the application of Zincite as an internal standard, were followed here, *e.g.* for the estimation of the amorphous content.

X-ray diffraction – Rietveld refinement and quantitative phase analysis. In order to quantify the phases observed and determine their lattice parameters and the degree of disordering, the Rietveld method was applied. The arrangement of the layers in the *c* direction of the LDH compounds synthesized showed no long-range ordering, *i.e.* the respective stacking sequences of the ordered hexagonal (ABAB) and trigonal LDH end-members (ABCABC) were randomly distributed.

https://doi.org/10.1346/CCMN.2013.0610503 Published online by Cambridge University Press

The analysis was carried out using the *BGMN* software which is able to evaluate parameters of the real structure such as the randomized stacking sequences of the layers in LDHs (Ufer *et al.*, 2008; Curtius *et al.*, 2009). This feature is based on a recursive approach which has been developed by Treacy *et al.* (1991) and implemented in the *DiFFaX* software package. This program simulates XRD patterns of compounds which exhibit virtual stacking faults and has been applied widely in the characterization of LDH compounds (*e.g.* Faour *et al.*, 2012; Britto *et al.*, 2008; Prasanna *et al.*, 2007; Radha *et al.*, 2007; Thomas *et al.*, 2004). The stacking faults of the layers lead to anisotropic peak broadening in the XRD pattern as the long-range order perpendicular to the layers is not present. Therefore, the related *hkl* reflections will broaden. The model for the calculations is based on the structure given by Arakcheeva *et al.* (1996).

In a projection parallel to the *c* axis (Figure 1), one octahedral layer and the oxygen positions of CO_3^{2-} and H_2O are revealed. The Wyckoff positions are 3f and 3g referring to the space group $P\bar{6}2m$ (189) and could be occupied by both O^{2-} and Cl^-. The cations, which occupy the Wyckoff positions 4h and 2e, have been omitted for clarity. Due to ordering of the Mg and Al cations the octahedra are slightly distorted. This type of LDH belongs to the $2H_1$ polytype (Bookin and Drits, 1993).

The metal cations are six-fold octahedrally coordinated by hydroxides (transparent edge-sharing octahedra). Between chloride anions and water molecules (black and gray spheres, respectively) are the constituents of the interlayer. The respective color differentiation of the spheres refers to the different atomic, *i.e.* Wyckoff, positions occupied by oxygen and chlorine.

The transition from one octahedral layer to the next is described as a mirror operation carried out with a mirror plane being situated virtually in the interlayer. According to the nomenclature of Bookin and Drits (1993) the hexagonal structure is referred to as the $2H_1$ polytype. The respective layer sequence has the notation AC=CA=AC. Contrary to that, the trigonal structure represents the $3R_1$ polytype and the ordering of layers exhibits the sequence AC=CB=BA=AC. The capital letter notation "A", "C", and "B" denotes the sites in which the hydroxyl anions of the octahedra reside. The = sign between adjacent layers indicates that the upper hydroxyl of the layer below and the lower hydroxyls of layer above form a prism and is, therefore, referred to as 'p-type.' If the minus sign is given, the respective hydroxyls form an octahedron. This arrangement is also referred to as 'o-type.'

The synthesis of this study exhibits a 3:1 ratio of the (*M*(II)/Al(III)) cations, which is observed in $3R_1$ polytypes and the notation sequence is AC=CB=BA=AC. For this polytype the upper hydroxyls of the lower layer and the lower hydroxyls of the upper layer also form prisms. This polytype was described by Allmann and Jepsen (1969) and by Bellotto *et al.* (1996). The space group of this LDH is $R\bar{3}m$ (166). The metal cations *M*(II) and *M*(III) occupy, unlike the $2H_1$ polytype, the same Wyckoff position 3a. Due to this common position of the different cations, the surrounding octahedra are not distorted, *i.e.* are identical considering the atomic positions, bond distances, and angles. The position of the interlayer oxygens of the CO_3^{2-} anion easily triggers the formation of hydrogen bonds to the adjacent hydroxyls when the arrangement of the related layers follows the p-type (Rives, 2001). This site occupancy of the cations is the same as that given by Allmann and Jepsen (1969) and Bellotto *et al.* (1996). The layer transition of two adjacent octahedral layers for this LDH type, referred to as $3R$ type, is described as a 2/3 shift parallel to the *a* and 1/3 parallel to the *b* axis. Following the notation of Bookin and Drits (1993) the respective layer sequence is AC=BA=CB=AC.

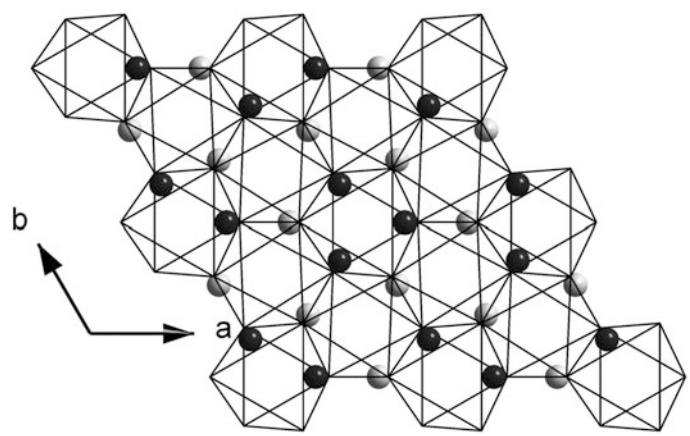

Figure 1. View down the *c* axis of the octahedral layer of the LDH (black solid lines). Hydroxyl groups have been omitted. Black and gray spheres represent the positions of chloride and water, respectively, in the interlayer. The depicted structure is in accord with Arakcheeva *et al.* (1996).

https://doi.org/10.1346/CCMN.2013.0610503 Published online by Cambridge University Press

In order to treat structural parameters more independently for the Rietveld refinement, the symmetry of the given structures which belong to the space groups $P\bar{6}2m$ (189) and $R\bar{3}m$ (166) were reduced to $P1$ (1). As the LDH syntheses being considered do not reflect exactly the structural properties of the applied model given by Arakcheeva *et al*. (1996), some further assumptions have been made for the calculation, *i.e.* the amount of Mg and Al and the *M*(II) site occupancy was a constraint on the stoichiometry listed in Table 1. Chloride and carbonate occupancies were also fixed for charge-balancing reasons. The stacking vectors which characterize the layer transition sequence were also fixed to 1/3, 1/3, 1 for the $3R_1$ type and to 0, 0, 1 for the $2H_1$ type. Hydrogen was not taken into account due to its very small contribution to the scattering power of the LDH compounds. The lattice parameters, the atomic positions of the interlayer water, the chloride, and the carbonate of the pure Mg-Al LDH were treated as restraints. This is also valid for the transition probability of the layers and the temperature factors which were considered to be isotropic. To account for the quality of the Rietveld refinements the ratio of R_{wp}/R_{exp} is given.

EXAFS measurements The samples were investigated as powders pressed without diluent into 7 mm-diameter pellets. Pellet preparation and measurements were done under inert gas. Four scans were performed for the Fe- and Co-bearing LDH and six scans for the Ni-doped LDH. All scans were recorded in transmission mode with an accumulation time of 2 s.

The accumulation time in the EXAFS range was increased by a factor square root of k, reaching its maximum at the end of the spectrum at k 16 $Å^{-1}$ with 8 s counting time.

The fits were performed simultaneously on the Fourier transform (FT) of the k^2-weighted $\xi(k)$ data and on the FT of k^3-weighted $\xi(k)$ data.

The Fe/Co/Ni K edge X-ray absorption fine structure (EXAFS) spectra were recorded at the INE-Beamline at ANKA (located in Karlsruhe, Germany (Rothe *et al.*, 2012) – the storage ring is operated at 2.5 GeV with a current of 180 mA). The spectra were energy calibrated to the first inflection point in the XANES of a Fe/Co/Ni metal foil (7.112/7.709/8.333 keV, respectively) and measured simultaneously. The EXAFS signal was recorded at room temperature in transmission mode using N_2-filled ionization chambers at ambient pressure. Si<111> crystals were used in the double crystal monochromator, operating in fixed-exit mode. The parallel alignment of the crystal faces was detuned to ~70% of the maximum beam intensity at the beginning of each scan. The incident intensity was then held constant by means of a piezo-driven feedback system to the second crystal.

The EXAFS fits were performed using *Artemis*, a program of the *IFEFFIT* package (Newville, 2001), using phase and amplitude data calculated for a 128 atom cluster (~8 Å diameter size, centered on the individual metal cations) and based on the modified model of Belloto *et al.* (1996), where the carbonate groups in the interlayer space were simply replaced by chloride. Among the possible occupation sites for Cl^- in the interlayer, four were represented. For Cl atoms, single-path scattering files for phase and amplitude were used. For the Ni- and Co-doped compounds, the multiple scattering paths (MS) for the first oxygen shell were taken into account in the fit. The k-range used in modeling was [4.2–14.7 $Å^{-1}$] for Ni-doped Cl-LDH, [4.2–14.2 $Å^{-1}$] for Co-doped Cl-LDH, and [3.4–11.4 $Å^{-1}$] for Fe-doped Cl-LDH. All fits were performed in the R-space simultaneously on the k^2- and k^3-weighted data.

Thermodynamic description of LDH solid solution–aqueous solution systems

Estimations of the molar Gibbs free energies, G_f, at 25ºC and 70ºC of the LDH solids were performed in order to investigate the effect of Fe-, Ni-, and Co-substitution into the Mg-Al-containing LDH on the aqueous solubility. Possible effects of oversaturation in the aqueous phases after synthesis were ignored and equilibrium between the precipitated solids and their corresponding 'synthesis' solutions was assumed.

To estimate the values of the Gibbs free energies of the solids, the following scheme was applied: (1) the speciation of the aqueous solutions obtained from the synthesis experiments was modeled for 70ºC using the Davies model (Davies, 1962) for aqueous electrolytes

Table 1. Stoichiometric formulae, cationic ratios of the synthesized LDHs, and estimates for molar Gibbs free energies of formation at 70ºC.

Stoichiometric formulae	M(II)/M(III)*	M(II)/M(III)**	G_f(343K)*** (kJ/mol)
$[Mg_3Al_1(OH)_8]Cl_{0.88}(CO_3)_{0.060}\cdot 2.40H_2O$	3.000	2.988	–3629.65
$[Mg_{2.9}Fe_{0.097}Al_1(OH)_{7.954}]Cl_{1.04}\cdot 2.70H_2O$	2.997	2.883	–3612.74
$[Mg_{2.9}Co_{0.100}Al_{1.01}(OH)_8]Cl_{1.03}\cdot 2.25H_2O$	2.970	2.911	–3604.67
$[Mg_{2.9}Ni_{0.090}Al_{0.99}(OH)_{7.86}]Cl_{1.09}\cdot 2.64H_2O$	3.020	2.926	–3593.14

* results obtained from ICP-OES analyses; ** results obtained from EDX measurements; *** results are presented for 'water-free' stoichiometries

https://doi.org/10.1346/CCMN.2013.0610503 Published online by Cambridge University Press

and Gibbs free energy minimization software GEM-Selektor (Kulik *et al.*, 2013), which includes the built-in NAGRA-PSI and SUPCRT/Slop98 chemical thermodynamic databases (Hummel *et al.*, 2002; Shock *et al.*, 1997). (2) From the calculated chemical potentials of Mg^{2+}, Ni^{2+}, Co^{2+}, Fe^{2+}, Al^{3+}, Cl^{-}, and OH^{-} species in the aqueous phase and from the measured stoichiometric compositions of the synthesized solids, the molar Gibbs free energies of formation of water-free compositions were calculated from the following equilibrium equation:

$$G_f = a\cdot\mu(Mg^{2+}) + b\cdot\mu(Me^{2+}) + c\cdot\mu(Al^{3+}) + d\cdot\mu(OH^{-}) + e\cdot\mu(Cl^{-}) \quad (1)$$

where Me^{2+} = Fe^{2+}, Ni^{2+}, or Co^{2+}, μ is the calculated chemical potential of the bracketed aqueous species, and indexes *a* to *e* are the stoichiometric coefficients, obtained from the chemical analyses of the solids synthesized.

RESULTS AND DISCUSSION

Characteristics of LDHs

The characterization of the pure Mg-Al-LDH was presented by Curtius and Kattilparampil (2005). Data obtained for the Fe-, Co-, and Ni-bearing LDHs are summarized (Table 1). The corresponding compositions of the supernatant liquids were also analyzed (Table 2). The amounts of Mg, Al, Fe, Co, Ni, and Na in the solids and their concentrations in aqueous solution after synthesis were determined by ICP-OES with an analytical error of ±5% (standard solutions were used in order to determine the deviation). The EDX technique (error range of ±1−6%) was applied to achieve greater accuracy with respect to the stoichiometry. The chloride in aqueous solutions and in the solids was determined photometrically (analytical error of ±5%). For the Fe-bearing LDH, the amount of Fe(III) was determined to be 5 wt.% by formation of a thiocyanate complex and this value is within the error range. Note that these measurements were performed using 'freshly prepared' Fe-bearing LDHs. An aliquot of this solid was sent to Karlsruhe (ANKA Beamline) for EXAFS measurements. The solid was stored for 8 weeks before measurement and, during that period, oxidation of Fe(II) could not be ruled out, although the sample was stored in a glass tube under argon atmosphere. Thermogravimetric analyses produced step-wise profiles having three main temperature regions, namely 50−260ºC, 260−500ºC, and 500−650ºC. The weight loss in the first step is related to the interlayer water. The second weight loss is due to the first step of dehydroxylation and the removal of chloride from the interlayer. Above 500ºC, the LDHs decompose and produce a mixture of metal oxides (Miyata, 1980). No differences were observed in the TGA curves of the Fe-, Co-, and Ni-bearing LDHs, indicating that the temperatures required for the removal of interlayer water, dehydroxylation of the cationic layers, and removal of interlayer anions were similar regardless of cation substitution. The thermal stabilities of Fe-, Co-, and Ni-bearing LDHs are, therefore, also similar.

Fourier-transform infrared spectroscopic measurements showed strong hydroxyl stretching bands (3460 cm^{-1}) and interlayer water bending bands (1636 cm^{-1}). In the fingerprint region (1090 cm^{-1}−550 cm^{-1}) the metal−O vibration bands were detected. All spectra showed a very weak adsorption band due to adsorbed CO_3^{2-} at 1352 cm^{-1}. The KBr pellets were produced under air and the carbonate ion had the greatest affinity for the LDHs (Miyata and Kumura, 1973).

Qualitative evaluation of the XRD measurements

The XRD patterns of the samples investigated (Figure 2) were quite similar and could be clearly identified with LDH compounds. Besides Zincite, which was added as an internal reference, no indications of other crystalline phases were observed.

To explain the peak shifts due to the incorporation of Fe, Co, and Ni in the LDH structure, a displacement-error correction by a Kα1/α2 stripping of the XRD patterns on the basis of the Zincite PDF-2-entry 00-036-1451 (cross symbols) was carried out. The stripping helped to overcome difficulties in the determination of peak positions by peak overlapping.

The XRD peaks from the synthesized LDH phases were broadened (Figure 2) due to the statistical distribution of the layer sequences of the 2*H* and 3*R* polytypes. The hexagonal 2*H* type is typical of the mineral manasseite (Arakcheeva *et al.*, 1996) and the 3*R* type, of hydrotalcite (Allmann and Jepsen, 1969; Bellotto *et al.*, 1996). This disordering could be

Table 2. Compositions of aqueous solutions (pH = 10.00 ± 0.02) after syntheses at 25ºC and 70ºC.

T (ºC)	Mg	Al	Fe	Ni	Co	Na	Cl	Corresponding synthesized solid
			μmol/kg			mmol/kg		
25	70.70	1.11	Below DL	–	–	90.16	117.70	Mg-Al-LDH
70	1.73	88.95	0.53	–	–	904	900	Mg-Al-Fe-LDH
70	34.10	1.85	–	–	1.36	903	900	Mg-Al-Co-LDH
70	1.89	9.64	–	1.19	–	903	900	Mg-Al-Ni-LDH

https://doi.org/10.1346/CCMN.2013.0610503 Published online by Cambridge University Press

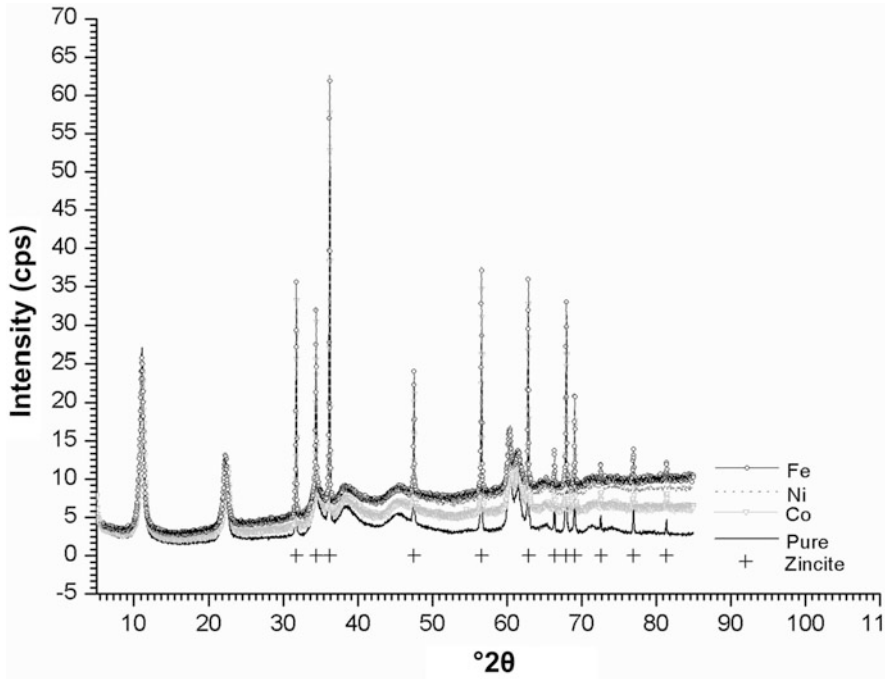

Figure 2. XRD patterns of LDH of Mg/Al (solid black), Fe (dashed gray), Co (dotted light gray), and Ni (dotted dark gray).

observed in the distinct asymmetric peak broadening of the reflections at 39 and 46º2θ. Yet the stacking faults do not have a strong impact on the *c* parameter. The interlayer distance in the *c* direction is not affected by this disordering and, thus, the 00*l* basal reflections at ~11 and 22º2θ do not suffer from peak overlap and exhibit a full-width at half maximum (FWHM) of ~0.5–0.7º2θ.

In order to assess the impact on the shift of the *a* and *c* lattice parameters due to the incorporation of the small amounts of Co (dotted light gray), Fe (dashed gray), and Ni (dotted dark gray) in the octahedral layer, the peak shift of 00*l* and 110 were evaluated, as, from these reflections, the lattice parameters could be derived directly (Figure 3a,b). The black XRD patterns refer to the pure Mg-Al-LDH compound.

The lattice parameters obtained by the Rietveld refinement were ~0.03 Å smaller than those determined manually (Table 3), a difference which may be explained by the FPA which has been applied in the evaluation of the *c* parameter.

Generally speaking, at low 2θ angles, the impact of the device function on the peak shape is greater than at higher angles (Klug and Alexander, 1974), leading to an overestimation of the *c* parameter.

The value of the *c* parameter was largest in the pure Mg-Al-LDH, was slightly less in the Co- and Ni-containing LDH, and was least in the Fe-containing LDH. Analogous decreases were also observed for the *a* parameter. By considering the ionic radius (Shannon, 1976, Table 3) of Fe(II), Fe(III), Co(II), Ni(II), Mg(II),

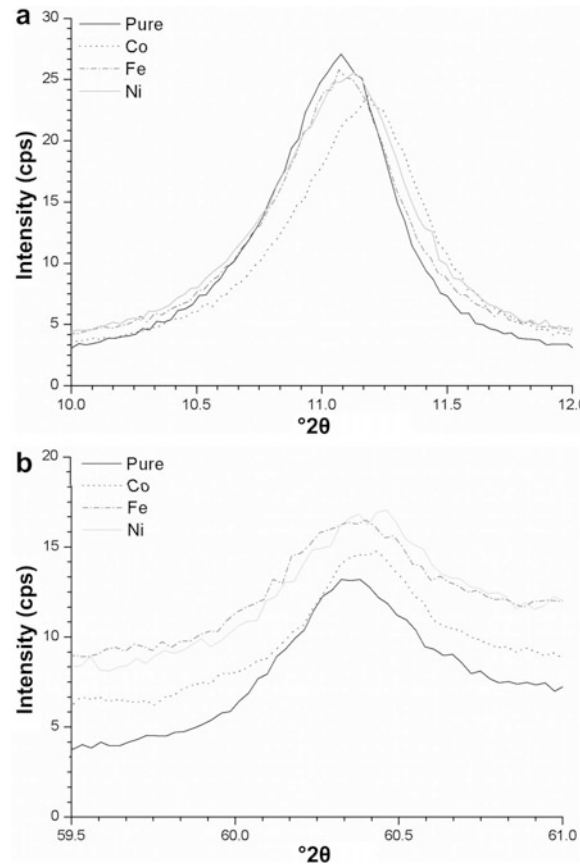

Figure 3. Alteration of the LDH lattice parameters *c* (a) and *a* (b) due to the substitution of Mg(II) by Co(II) (dotted light gray), Fe(II) (dashed gray), and Ni(II) (solid light gray).

https://doi.org/10.1346/CCMN.2013.0610503 Published online by Cambridge University Press

Table 3. XRD analysis of the LDHs and interlayer water analysis by TGA.

LDH type/ r(x) (Å) [SHA 76]	a (Å)	c (Å)	Octahedral elongation c (Å)	R_{wp}/R_{exp}	Transition $3R/3R$, (%)	Zincite weighed (%)	Zincite calc. (%)	Interlayer H_2O TGA analysis	Interlayer H_2O calc.	Density (g/cm^3)
Fe(III) LDH rFe(III) = 0.645	3.0630±0.0005	7.8949±0.0019	2.1461±0.0066	1.73	50.51±0.27	10.200	9.876±0.016	2.700	2.765±0.016	1.979
Ni LDH rNi(II) = 0.69	3.0636±0.0006	7.9492±0.0023	2.1328±0.0070	1.96	49.71±0.32	10.010	9.755±0.014	2.640	2.617±0.018	1.876
MgAl LDH rMg(II)= 0.72 rAl(III) = 0.535	3.0649±0.0007	7.9710±0.0028	2.1377±0.0074	2.70	54.03±0.41	9.990	9.579±0.025	2.400	2.959±0.023	1.881
Co LDH rCo(II) = 0.745	3.0646±0.0005	7.9552±0.0021	2.1503±0.0075	1.83	50.67±0.37	10.080	9.686±0.031	2.250	2.744±0.021	1.903
Fe(II) LDH rFe(II) = 0.78	3.0630±0.0005	7.8947±0.0020	2.1407±0.0068	1.78	50.71±0.29	10.200	9.927±0.016	2.700	2.867±0.020	1.923

and Al(III) and its effect on the lattice parameters, the observed decrease in the Fe-LDH may be explained by the relatively low radius of Fe(III).

In order to estimate the Fe(II)/Fe(III) ratio, the respective occupancy density for these cations was calculated using the Rietveld method by introducing Fe(III) into the Fe(II) atomic position. The additional positive charge introduced by Fe(III) was compensated by carbonate, which was, therefore, assumed to be present due to sample alteration by the oxidation of Fe(II). The outcome of this calculation showed that Fe(III) can occupy completely the atomic position of Fe(II). The R_{wp}/R_{exp} ratio improved slightly (Table 3) but, considering the small admixtures of iron, no shift of any significance in the a or c parameters was observed. These data were insufficient, however, to determine whether the sites were occupied by Fe(II) or Fe(III). The Fe concentrations used, equivalent to only 1/30 of the amount of Mg(II), were quite small. Reliable statements regarding the presence of Fe(III) due to oxidation of Fe(II) may only be made after analyzing solid solutions of LDH compounds having greater Fe concentrations.

During the refinement, elongation of the octahedral layer in the c direction was also computed. According to Rives (2001) this parameter, which describes the octahedral flattening perpendicular to the c axis, should become smaller as the radius of the metal cations increases.

The trend of increasing ionic radii (Shannon, 1976) of Fe(III) < Ni(II) < Mg(II) and Co(II) < Fe(II) failed to yield a corresponding elongation of the octahedra in the c direction, which remained constant, thus showing a clear lack of dependency on the ionic radius. This observation may be attributed to the small concentrations of the metal cations despite their different ionic radii. Note also that this calculated parameter (*hc)* for the elongation exhibits a value which is generally ~0.1 Å larger than the reported distances (Arakcheeva *et al.*, 1996; Allmann and Jepsen, 1969; Bellotto *et al.*, 1996). Whether this observation could be attributed to the large amount of stacking faults (Table 3) or to any other cause has yet to be clarified.

With respect to the stacking faults, all the LDHs investigated exhibited a transition probability of ~50% (Table 3), which means that the probability of adjacent layers in the c direction being a 3R type or a 2H type is 50%.

The calculated amounts of interlayer water were in good agreement with those determined by thermogravimetric analysis. The small deviations of these values from the chemical formulae of the different LDHs (Table 3) could be attributed to exposure to the atmosphere during the addition of the internal standard.

The amount of interlayer water could have an effect on the c parameter, *i.e.* the pure Mg-Al-LDH has the largest amount of interlayer water and exhibits the largest c parameter. The application of different

https://doi.org/10.1346/CCMN.2013.0610503 Published online by Cambridge University Press

humidities during XRD measurements could help evaluate and clarify the related impact.

Generally, the calculated X-ray densities (see Table 3) were in excellent agreement with the theoretical value of 1.87 g/cm^3. The latter calculation was based on an assumed chemical composition $[Mg_{2.25}Al_{0.75}(OH)_6]\cdot Cl\cdot 3H_2O$ of the LDH exhibiting lattice parameters of 3.05 Å and 23.85 Å for the *a* and *c* axes, respectively.

A Rietveld refinement of the Ni-bearing LDH (the pure Mg-Al-LDH and the Co-, Fe-containing LDHs are not presented) was performed (Figure 4). By simple visual inspection, the applied structural model for the LDH syntheses fits the measured XRD patterns very well. The R_{wp}/R_{exp} ratios are in the same range from 1.73 to 1.96 for the LDH synthesis doped with Fe, Ni, and Co. The equivalent ratio for the pure Mg-Al-LDH is slightly increased (Table 3). In order to clarify the incorporation of cations of different radius, synthesis of a solid-solution series with increased concentrations should be carried out.

The structural properties of LDHs also depend on the identity and quantity of constituents in the interlayer, *e.g.* the water content may be altered when the samples are prepared for X-ray analysis. The possibility that carbonate was incorporated cannot be ruled out. Such alterations must, therefore, be considered as restraints, *i.e.* as parameters which are allowed to vary within predefined intervals in the structural model being applied for the Rietveld analysis. If the starting values and the related intervals are not well constrained, the optimization calculations within the Rietveld method could possibly end up with values which may not reflect sound structural properties. Furthermore, as the LDH samples considered suffer from distinct stacking faults, providing a suitable structure model which considers the loss of the long-range ordering of lattice constituents in crystalline samples is challenging.

EXAFS

Interatomic distances and coordination numbers can be determined by EXAFS measurements. For a pure Mg-Al-LDH, taking the metal cation as the center, the interatomic distances for the nearest coordination shells are summarized in Table 4. For comparison, the distances of the nearest coordination shells are given for the fougerite structure, $(Fe(OH)_2)(OH)_{0.25}(H_2O)_{0.5}$ (Trolard *et al.*, 2007), a LDH analogue compound where the Mg/Al is replaced completely by Fe with an Fe(II)/Fe(III) ratio = 3.

The FT magnitude taken in the range 3.2–13.5 Å^{-1} for all samples (Figure 5) and the EXAFS (Figure 6) signals recorded for the Ni- and Co-bearing LDHs were very similar. The compounds seemed to have a well organized structure as neighbor contributions can still be seen at ~6 Å (5.6 Å in the FT which has not been phase-shift corrected). On the contrary, the EXAFS signal for the Fe-doped LDH and its FT differed significantly compared with the spectra of samples doped with Ni or Co.

Firstly, the FT peak at ~6 Å was no longer visible, and useful information seemed to end near 3.0 Å in the FT. In addition, the O first shell FT peak was at a smaller distance than for Ni/Co; it was expected at a similar or slightly longer distance as given by the valence-bond theory: in coordination 6, Fe(II)–O is expected at 2.14 Å, Co(II)–O at 2.10 Å, and Ni(II)–O at 2.06 Å (Brown and Altermatt, 1985).

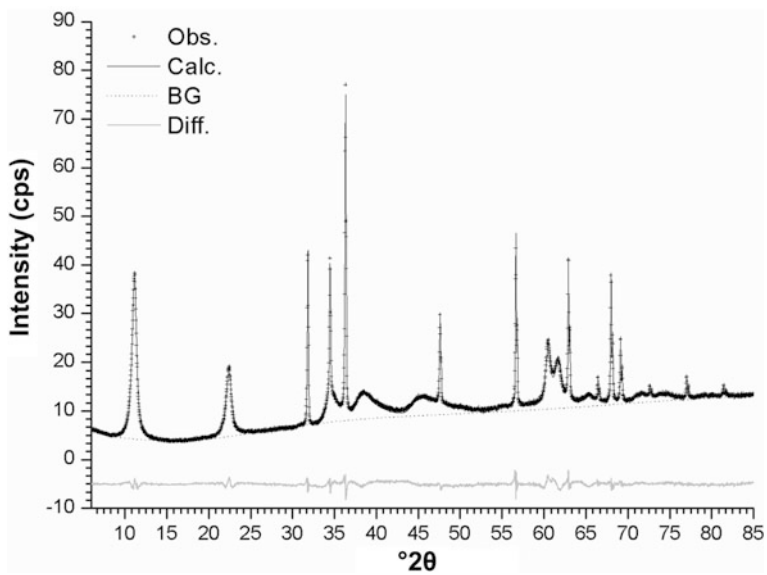

Figure 4. Rietveld plot of the Ni-doped LDH with background (BG).

https://doi.org/10.1346/CCMN.2013.0610503 Published online by Cambridge University Press

Table 4. Metric parameters (R = distances, N = coordination numbers) of LDH with a metal cation as the center. Distances are given for Mg-Al LDH (left) and for fougerite (right).

Back-scatterer	N	R (Å)	Back-scatterer	N	R (Å)
O	6	2.01	O	6	2.09
Mg/Al	6	3.05	Fe	6	3.19
O	6	3.65	O	6	3.82
Cl*	1	3.79/4.18/4.86/5.17/6.00	Cl*	1	4.15−4.70/5.65−6.38
O	12	4.76	O	12	4.97
Mg/Al	6	5.28	Fe	6	5.53
Mg/Al	6	6.09	Fe	6	6.38
O	12	6.42	O	12	6.71

* five positions established among all possible positions for Cl^-/CO_3^- in the interlayer.

The complete predictions for oxidation states +II and +III in coordinations 4 and 6 were summarized (Table 5), and the fitted results obtained for the Ni-, Co-, and Fe-bearing LDHs were compiled (Table 6).

During the fit, the overall scaling factor, S_0^2, was varied and the coordination numbers, N, were fixed to the expected values. The R factor of the fit yielded a 0% residual disagreement between fitted and experimental data for Ni, 0.4% for Co, and 0.1% for Fe.

This similarity between the Ni and Co solids was confirmed by the structural parameters obtained. For both Ni- and Co-doped LDHs, the data were well reproduced using nine shells in the FT range [1.25−6.20 Å] for Ni and [1.09−6.20 Å] for Co (Figures 5, 6).

The first shell distance was slightly greater for Co (2.08 Å) than for Ni (2.04 Å). These distances matched well the distance predicted by the valence-bond theory for a metal cation having an oxidation state of +II in six-fold coordination.

These distances were also longer than in the Mg-Al LDH (2.01 Å), where the distance was averaged statistically between Mg−O (2.10 Å) and −Al−O (1.88 Å). This reflects the smaller 'mean ionic radius' (0.67 Å) obtained for a statistic distribution of Mg (0.72 Å) and Al (0.54 Å) in the undoped LDH compared to ionic radii of Ni(II) or Co(II) ($\geqslant$0.69 Å). The first cation shell distances for Mg or Al (cannot differentiate between them) were perfectly compatible with the LDH structure for Ni (3.05 Å) and for Co (3.08 Å). The only significant difference between the Ni and Co samples was in the position of the second cation shell (5 × Mg/Al+1 × Ni or Co) which was located at the same distance as for pure LDH in the case of Co and 0.16 Å farther for Ni.

For Fe-doped Cl-LDH, only three shells were needed to reproduce the data over a shorter FT range [1.13−3.15 Å] (Figures 5, 6). A first coordination sphere with 6 oxygen atoms at 2.00 Å with a Debye-Waller factor (σ^2)

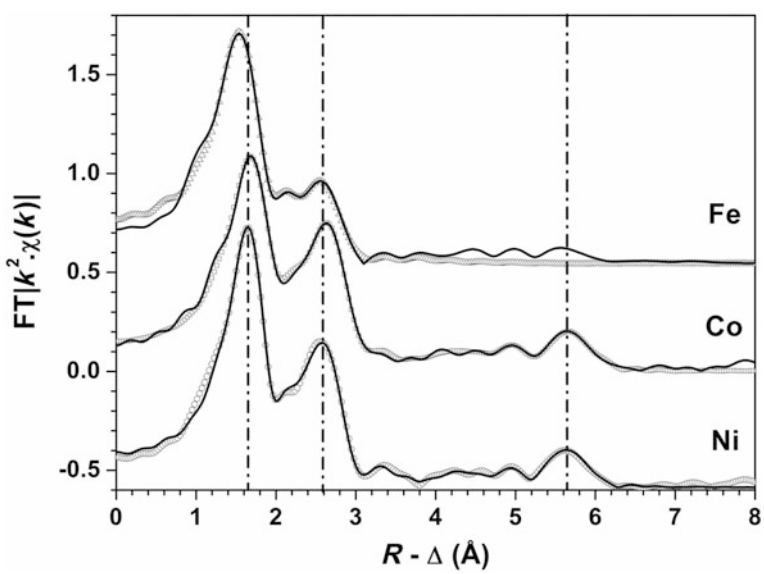

Figure 5. Fourier Transform (FT) magnitude (thick solid line) and fitted result (open triangles for Fe, open squares for Co, and open circles for Ni) with FT taken in the range 4.2−14.7 $Å^{-1}$ for Ni (lower), 4.2−14.2 $Å^{-1}$ for Co (middle), and 3.4−11.4 $Å^{-1}$ for Fe (upper) as used for the fit .

https://doi.org/10.1346/CCMN.2013.0610503 Published online by Cambridge University Press

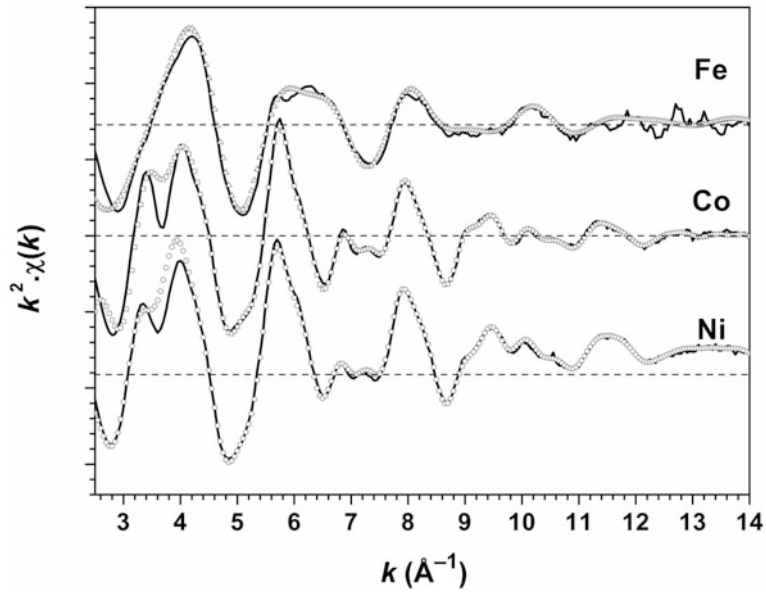

Figure 6. k^2-weighted EXAFS of the sample (solid line) and its fitted results (open triangles for Fe, open squares for Co, and open circles for Ni) for all three samples.

of 7.28 Å^2 was obtained. This bond distance was far from that expected for Fe(II) in octahedral coordination (Table 5) or as found for six-fold coordinated Fe(II) in the literature (2.16 Å in FeO (ICSD 82233)). Even in the case of fougerite (Fe-containing LDH), where the crystal-structure parameters account for both Fe(II) and Fe(III) (ratio 3:1) in octahedral positions, the mean value was found to be 2.09 Å (crystal-structure data by Trolard *et al.*, 2007).

Table 5. Bond distances expected according to the valence-bond theory predictions. The relationship between bond length (R) and bond valence (s) is: $s = \exp((Ro-R)/B)$ where Ro and B are valence-bond parameters that depend on the two atoms forming the bond (Brown and Altermatt, 1985). B is 0.37. CN: coordination number.

Cation−O	CN	R (Å)	Ro (Å)
Ni(II)	4	1.91	1.654
	6	2.06	
Co(II)	4	1.95	1.692
	6	2.10	
Fe(II)	4	1.99	1.734
	6	2.14	
Ni(III)	4	1.74	1.74
	6	1.89	
Co(III)	4	1.79	1.70
	6	1.94	
Fe(III)	4	1.87	1.759
	6	2.01	
Mg(II)	6	2.10	1.693
Al(III)	6	1.88	1.620

Such a short bond distance can be achieved either by Fe(II) in tetrahedral or Fe(III) in octahedral coordination. The LDH or fougerite structure does not allow for tetrahedral sites. Study by XRD of the present samples gave no evidence for the presence of crystalline phases other than LDH. Furthermore, the Fe-K EXAFS intensity did not match the four-fold oxygen coordination. The presence of Fe(III) in the octahedra was likely as it occurred in fougerite and in the LDH at the position of trivalent cations (Al(III)). In addition, the presence of trivalent Fe, suggested by the EXAFS analysis, was confirmed by the XANES analysis (Figure 7).

Most of the Fe was in oxidation state +III as the edge position matched perfectly that of Fe(III). The first derivative of the signal (Figure 7b) revealed a smaller amount of Fe(II) which was invisible in the original signal. The inset shows an enlargement of the characteristic feature for the 1s → 3d/4p transition (Wilke *et al.*, 2001; Fink *et al.*, 2012) confirming that no Fe(II) was detected, and that Fe occurred as Fe(III) in the Fe-doped Cl-LDH.

With respect to the first cation Mg/Al shell, the determined distance of 3.08 Å for the Fe-bearing LDH is perfectly compatible with the LDH structure. The presence of another Fe(III) located in the next direct octahedral shell forming an Fe(III)-Fe(III) pair, where the octahedra share an edge, was observed. This was not the case for Ni(II) and Co(II) cations where the next Ni/Co was farther away.

Estimation of Gibbs free energies of LDHs

The molar Gibbs free energies of the precipitates were calculated by assuming a thermodynamic equilibrium between solids (Table 1) and corresponding

https://doi.org/10.1346/CCMN.2013.0610503 Published online by Cambridge University Press

Table 6. Metric parameters (R = distances, N = coordination numbers, σ^2 = EXAFS Debye-Waller factors, ΔE_0 = relative energy shifts held as global parameters for like atoms) from least-squares fit analysis of FT data.

Sample	Back-scatterer	R (Å) (±0.02 Å)	N fixed	σ^2 (Å^2) × 10^{-3}	δE_0 (eV)	Goodness of fit (%)
	O	2.05	6	5.82	−1.0	
	Mg/Al	3.05	6	6.84	−1.8	
	O	3.55	6	12.1	−1.0	
Ni-doped Cl-LDH	O	4.78	12	20.0	−1.0	
	Ni	5.39	1	4.85	−0.0	0.20
S_0^2 = 0.84 ± 0.03	Mg/Al	5.43	5	21.8	−1.9	
	Cl	5.84	1	3.25	−0.8	
	Mg/Al	6.21	6	3.83	−1.9	
	O	6.41	12	5.48	−1.0	
	O	2.08	6	7.88	+1.7	
	Mg/Al	3.08	6	6.64	+2.5	
	O	3.57	6	12.2	+1.7	
Co-doped Cl-LDH	O	4.76	12	21.8	+1.7	
	Co	5.19	1	4.60	+2.1	0.40
S_0^2 = 0.85 ± 0.04	Mg/Al	5.27	5	5.80	+2.5	
	Cl	5.88	1	1.97	+2.6	
	Mg/Al	6.24	6	3.82	+2.5	
	O	6.43	12	4.78	+1.7	
	O	2.00	6	7.28	−1.3	
Fe-doped Cl-LDH	Mg/Al	3.08	5	8.28	−0.4*	0.14
S_0^2 = 0.69 ± 0.05	Fe	2.94	1	9.00	−0.4*	

* parameters are constrained to the same value.

mother liquor (Table 2). Using the GEM-Selektor (Kulik *et al*., 2013) as described above, the compositions of liquids were modeled and the chemical potentials of the dissolved compounds calculated. The estimates demonstrated the effect of (1) intercalation of different anions (*i.e.* chloride and carbonate) in the interlayer space and (2) isostructural incorporation of various divalent cations (*i.e.* Fe^{2+}, Co^{2+}, Ni^{2+}) in the brucite-like layers, on the aqueous solubility of LDHs.

The effect of intercalated anion

The effect of intercalation of CO_3^{2-} and Cl^- anions in the interlayer space of the LDH has been investigated by comparing the estimated values of the formation constants. In the first step, the value of the Gibbs free energy of formation (−3619.14 kJ/mol) obtained for a pure 'water-free' $Mg_3Al(OH)_8Cl_1$ LDH at 25ºC was used. Then, the reaction of formation of this composition from the aqueous species was formulated:

$$3Mg^{2+}_{(aq)} + Al^{3+}_{(aq)} + 8OH^-_{(aq)} + Cl^-_{(aq)} = Mg_3Al(OH)_8Cl \quad (2)$$

The value of the Gibbs free energy of this reaction ($\Delta_r G$) was calculated using the standard Gibbs free energies of the aqueous species $Mg^{2+}_{(aq)}$ (−453.99 kJ/mol), $Al^{3+}_{(aq)}$ (−483.71 kJ/mol), $OH^-_{(aq)}$ (−157.27 kJ/mol), and $Cl^-_{(aq)}$ (−131.29 kJ/mol) from the NAGRA-PSI database (Hummel *et al.*, 2002). Finally, the fundamental relationship $\Delta_r G = -RT\cdot\ln K$ has been used in order to obtain the value of the formation constant for the LDH composition at 25ºC.

The same scheme was applied to calculate the formation constant for the carbonate-bearing LDH composition $Mg_3Al(OH)_8(CO_3)_{0.5}$ with G^o_{298} = −3746.90 (Rozov *et al.*, 2011). The formation of the LDH was represented as:

$$3Mg^{2+}_{(aq)} + Al^{3+}_{(aq)} + 8OH^-_{(aq)} + 0.5CO^{2-}_{3\,(aq)} = Mg_3Al(OH)_8(CO_3)_{0.5} \quad (3)$$

where $G^o_{298}(CO_3^{2-})$ = –527.98 kJ/mol (Hummel *et al.*, 2002).

The observed difference between the formation constant of the CO_3^{2-}-bearing LDH (logK = 66.45) and the Cl^--bearing LDH (logK = 67.29) denotes the effect of the intercalated anion, demonstrating that Cl-containing LDHs are more soluble than carbonate-containing types. This result is in agreement with previous data of Allada *et al.*, (2005), who performed calorimetric measurements and predicted greater solubility of chloride-containing LDHs in comparison with carbonate-containing substances.

The effect of substituted cations

The Gibbs free energies of formation were calculated for the synthesized LDHs which include Fe(II), Co(II), and Ni(II) cations in the brucite-like layers. Note that at the present stage of this study, estimation of the

https://doi.org/10.1346/CCMN.2013.0610503 Published online by Cambridge University Press

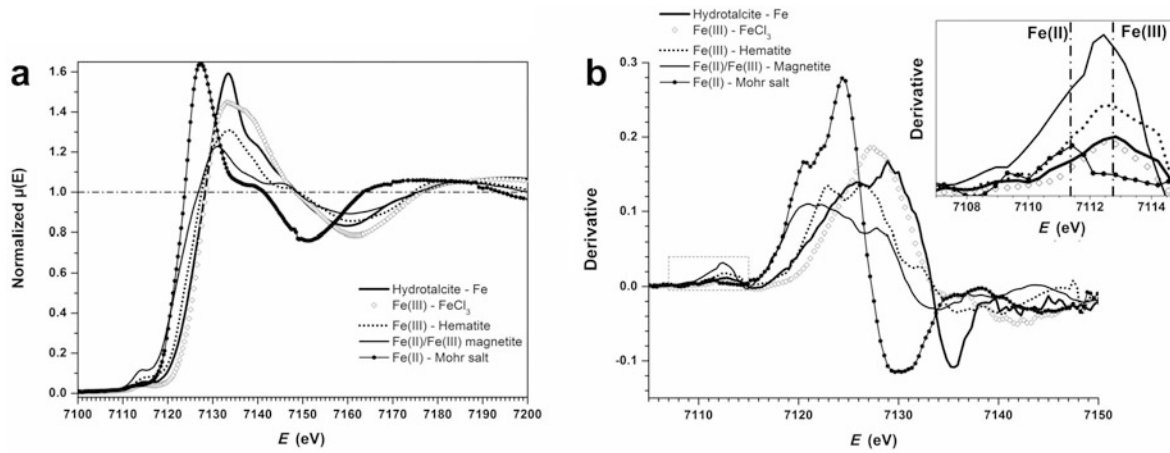

Figure 7. (a) Comparison of the normalized XANES profile for different reference samples (hematite and $FeCl_3$ for pure Fe(III), Mohr salt for pure Fe(II), and magnetite for mixed Fe(II)/Fe(III)) with the Fe Cl-LDH. (b) Comparison of the first derivative of the XANES signal shown for the reference samples and Fe Cl-LDH with the characteristic feature for the 1s → 3d/4p transition in the inset.

formation constants for Fe(II)-, Co(II)-, and Ni(II)-containing compositions was not performed because the standard thermodynamic properties of these substances are unknown. First, no reliable database exists of the standard entropies, enthalpies, and heat capacities of these substances. Second, the calculations performed were done for the conditions during syntheses only (*i.e.* T = 70ºC, P = 1 bar). The estimated Gibbs free energies (Figure 8, Table 1) at 70ºC correlate strongly with the ionic radii (Shannon, 1976) of the substituting cation in octahedral coordination (r^{2+}_{Fe} = 0.78 Å; r^{2+}_{Co} = 0.745 Å; r^{2+}_{Ni} = 0.69 Å), demonstrating that the stabilities of LDHs depend heavily on the type of substituting divalent cation.

A comparison of the estimated Gibbs free energy values for Fe(II), Ni(II), and Co(II)-doped solids with mole fraction (x^{2+}_{Me}) of Fe, Co, or Ni ≈ 0.1, with the Gibbs free energy of the pure CO_3^{2-}- and Cl^--containing LDH end-members (Figure 8) was performed. For this purpose the standard Gibbs free energy of a pure 'water-free' LDH (composition $Mg_3Al(OH)_8Cl_1$) was estimated at 70ºC using the data obtained from Rozov *et al.* (2011) (standard molar entropy 238.46 J/(mol·K), enthalpy −4161.19 kJ/mol, and heat capacity 324.20 J/(mol·K) at 25ºC for a CO_3^{2-}-bearing LDH with a stoichiometry of $Mg_3Al(OH)_8(CO_3)_{0.5}$). This process allows extrapolation of the data for G_f of a pure Cl^--containing LDH from 25ºC (−3619 kJ/mol) to 70ºC (−3629 kJ/mol) as well as

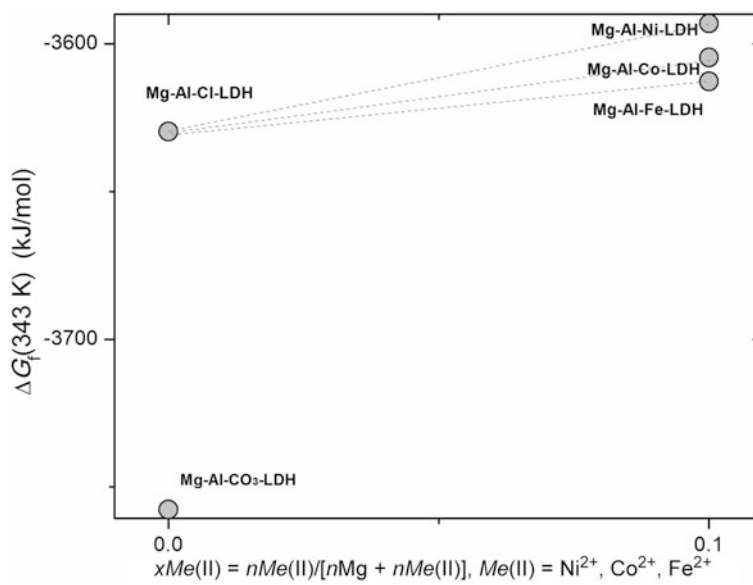

Figure 8. Gibbs free energies of 'water-free' pure Mg/Al-LDHs and Fe(II)-, Co(II)-, and Ni(II)-containing LDHs at 70ºC as a function of mole fraction of substituted cation in octahedral coordination.

https://doi.org/10.1346/CCMN.2013.0610503 Published online by Cambridge University Press

for a $Mg_3Al(OH)_8(CO_3)_{0.5}$ from 25ºC (−3746 kJ/mol) to 70ºC (−3757 kJ/mol).

The Gibbs free energies (Figure 8) of a pure Mg-Al-Cl-LDH and of a pure Mg-Al-CO_3-LDH are smaller than the values for Fe(II)-, Ni(II)-, and Co(II)-containing LDHs. Only the addition of 0.1 stoichiometric units of Fe(II), Co(II), and Ni(II) into the LDH structure increases the Gibbs free energy value to −3612±50, −3604±50, and −3593 ±50 kJ/mol, respectively, and explains the effect of the incorporation of various divalent metals into the structure on the aqueous solubility of LDHs.

The effect of the incorporation of divalent metals on the aqueous solubility of LDH phases observed is in agreement with the recent literature (Allada *et al.*, 2002). Based on calorimetric measurements of Ni(II)- and Co(II)-containing samples (Allada *et al.*, 2002), the calculated solubility constants increased with increased substitution of Ni(II) for Co(II) mole fractions. However, the change in solubility as Ni(II) substitutes for Co(II) exerts a relatively minor effect. The same point was confirmed in the present study. The difference between the Gibbs free energy values determined for Ni(II)- and Co(II)-containing LDH is ~11 kJ/mol, which is in the range of the estimated uncertainties. The results suggest that the difference in the solubility of Co- and Ni-containing phases will be scarcely distinguishable.

SUMMARY AND CONCLUSIONS

Mg-Al-Cl-bearing LDHs doped with Ni, Co, or Fe cations (the mole fraction of Ni, Co, and Fe ≈ 0.1) and the (Mg/Al, (Mg+Ni)/Al, (Mg+Co)/Al, and (Mg+Fe)/Al cationic ratios close to 3:1) have been synthesized successfully by the co-precipitation method. Analyses by PXRD and EXAFS were performed in order to characterize the structures of these LDHs. The PXRD results showed that all the samples were pure LDHs with each exhibiting distinct stacking faults (the 3*R*/2*H*-type layer stacking sequence determined was ~0.5). The estimated lattice parameters of Co-containing, Ni-containing, and pure Mg/Al LDHs were significantly different, as one might expect, taking into account the differences in the ionic radii of the different *M*(II) cations. The very small Co and Ni contents in these LDHs (*M*(II)/Mg ≈ 1:30) might explain this observation. The results of EXAFS measurements demonstrated similar structural features of Ni- and Co-bearing LDHs where Ni and Co atoms were incorporated as divalent cations in the LDH structure at octahedral crystallographic positions. The distances determined matched very well the distances predicted by the valence-bond theory for a metal cation in an oxidation state of +II in a six-fold coordination.

Unexpectedly, the smallest lattice parameters were observed for the Fe-bearing LDH. The EXAFS results indicated clearly the isostructural incorporation of Fe in the octahedral layers but as Fe(III) only. For the first coordination sphere with 6 oxygen atoms, a bond distance of 2 Å was obtained. Such a short distance can only be explained by Fe(II) in tetrahedral or by Fe(III) in octahedral coordination.

With XANES measurements, the presence of Fe(III) was confirmed and no Fe(II) was detected. Nevertheless, the presence of Fe(II) in amounts up to 5 wt.% cannot be ruled out. Indeed, information about the oxidation state of iron in synthesized Mg-Al-Fe-Cl-containing LDH is contradictory. With freshly prepared Fe-bearing LDH, only Fe(II) (using the thiocyanate complex reaction) was detected.

Thermodynamic modeling using the *GEMS-PSI* code package was performed in order to predict the behavior of different LDH compositions in aqueous media. Assuming that thermodynamic equilibrium was achieved between synthesized solids and solutions, the first estimates (−3593±50, −3604±50, −3612±50 kJ/mol) for the Gibbs free energies of formation of Mg-Al-Ni-Cl-, Mg-Al-Co-Cl-, and Mg-Al-Fe(II)-Cl-bearing LDHs at 70ºC were obtained. The incorporation of Fe, Co, and Ni within the LDH lattice revealed no impact on the aqueous solubilities of these LDHs, in good agreement with the data of Allada *et al.* (2002). Moreover, the estimated Gibbs free energies correlated with the ionic radii of substituting divalent cations, a finding which is useful in the prediction of thermodynamic properties and aqueous solubilities of LDHs with variable divalent cations. The influence of the interlayer anion on the aqueous solubilities of LDHs was investigated for carbonate (Rozov *et al.*, 2011) and chloride (present study) and carbonate-containing LDHs were shown to be significantly less soluble than analogous chloride-bearing substances.

ACKNOWLEDGMENTS

The authors are grateful to Nicolas Finck for providing the Fe reference data, and to the Synchrotron Light Source (ANKA) in Karlsruhe, Germany, for access to instruments at the beam lines. For financial support the authors thank the Bundesministerium für Bildung und Forschung (VESPA-project, Förderkennzeichen 02E10780).

REFERENCES

NAGRA technical report 02-05, Project Opalinus Clay. Demonstration of disposal feasibility for spent fuel, vitrified high-level waste and long-lived intermediate-level waste (entsorgungsnachweis). (2002), 02-05, NAGRA, Wettingen, Germany.

Abdelouas, A., Crovisier, J.L., Lutze, W., Fritz, B., Mosser, A., and Muller, R. (1994) Formation of hydrotalcite-like compounds during R7T7 nuclear waste glass and basaltic glass alteration. *Clays and Clay Minerals*, **42**, 526−533.

Allada, R.K., Navrotsky, A., Berbeco, H.T., and Casey, W.H. (2002) Thermochemistry and aqueous solubilities of hydrotalcite-like solids. *Science*, **296**, 721−723.

Allada, R.K., Pless, J.D., Nenoff, T.M., and Navrotsky, A. (2005) Thermochemistry of hydrotalcite-like phases intercalated with CO_3^{2-}, NO_3^-, Cl^-, I^-, and ReO_4^-. *Chemistry of*

https://doi.org/10.1346/CCMN.2013.0610503 Published online by Cambridge University Press

Materials, **17**, 2455–2459.
Allmann, R.J. and Jepsen, H.P. (1969) Die Struktur des Hydrotalkits. *Neues Jahrbuch für Mineralogie Monatshefte*, 544–551.
Arakcheeva, A.V., Pushcharovskii, D.Y., Rastsvetaeva, R.K., Atencio, D., and Lubman, G.U. (1996) Crystal structure and comparative crystal chemistry of $Al_2Mg_4(OH)_{12}(CO_3)_3{\cdot}(H_2O)$, a new mineral from the hydrotalcite-manasseite group. *KRISAJ*, **41**, 1024–1034.
Bellotto, M., Rebours, B., Clause, O., Lynch, J., Bazin, D., and Elkaïm, E. (1996) A reexamination of hydrotalcite crystal chemistry. *The Journal of Physical Chemistry*, **100**, 8527–8534.
Bergmann, J., Friedel, P., and Kleeberg, R. (1998) BGMN – a new fundamental parameters-based rietveld program for laboratory X-ray sources, its use in quantitative analysis and structure investigations. *CPD Newsletter*, 5–8.
Bookin, A.S. and Drits, V.A. (1993) Polytype diversity of the hydrotalcite-like minerals – I. Possible polytypes and their diffraction features. *Clays and Clay Minerals*, **41**, 551–557.
Bragg, W.L. (1913) The diffraction of short electromagnetic waves by a crystal. *Proceedings of the Cambridge Philosophical Society*, **17**, 43–57.
Britto, S., Thomas, G.S., Vishnu Kamath, P., and Kannan, S. (2008) Polymorphism and structural disorder in the carbonate containing layered double hydroxide of Li with Al. *Journal of Physical Chemistry C*, **112** (25), 9510–9515.
Brown, I.D. and Altermatt, D. (1985) Bond-valence parameters obtained from a systematic analysis of the inorganic crystal-structure database. *Acta Crystallographica Section B-Structural Science*, **41**, 244–247.
Cavani, F., Trifiro, F., and Vaccari, A. (1991) Hydrotalcite-type anionic clays: Preparation, properties and applications. *Catalysis Today*, **11**, 173–301.
Cui, D. and Spahiu, K. (2002) The reduction of U(VI) on corroded iron under anoxic conditions. *Radiochimica Acta*, **90**, 623–628.
Curtius, H., Kaiser, G., Paparigas, Z., Hansen, B., Neumann, A., Klinkenberg, M., Müller, E., Brücher, H., and Bosbach, D. (2010) Wechselwirkung mobilisierter Radionuklide mit sekundären Phasen in endlagerrelevanten Formationswässern. *Berichte des Forschungszentrums Jülich-4333*, ISSN 0944–2952.
Curtius, H. and Kattilparampil, Z. (2005) Sorption of iodine on Mg-Al-layered double hydroxide. *Clay Minerals*, **40**, 455–461.
Curtius, H., Ufer, K., and Dardenne, K. (2009) Preparation and characterization of Zr(IV)-containing Mg-Al-Cl layered double hydroxide. *Radiochimica Acta*, **97**, 423–428.
Davies, C.W. (1962) *Ion Association*. Pp. 41. Butterworths, London.
Faour, A., Mousty, C., Prevot, V., Devouard, B., De Roy, A., Bordet, P., Elkaim, E., and Taviot-Gueho, C. (2012) Correlation among structure, microstructure, and electrochemical properties of NiAl-CO_3 layered double hydroxide thin films. *Journal of Physical Chemistry*, **116**, 15646–15659.
Finck, N., Dardenne, K., Bosbach, D., and Geckeis, H. (2012) Selenide retention by mackinawite. *Environmental Science & Technology*, **46**, 10004–10011.
Hummel, W., Berner, U., Curti, E., Pearson, F.J., and Thoenen, T. (2002) Nagra/PSI chemical thermodynamic data base 01/01. *Radiochimica Acta*, **90**, 805–813.
Klug, H.P. and Alexander, L.E. (1974) *X-ray Diffraction Procedures*. Wiley-Interscience, New York.
Kulik, D.A., Wagner, T., Dmytrieva, S.V., Kosakowski, G., Hingerl. E.F., Chudnenko, K.V., and Berner, U. (2013) GEM-Selektor geochemical modeling package, revised algorithm and GEMS3K numerical kernel for coupled simulation codes. *Computational Geosciences*, **17**, 1–24.
Mazeina, L., Curtius, H., Fachinger, J., and Odoj, R. (2003) Characterisation of secondary products of uranium-aluminium material test reactor fuel element corrosion in repository-relevant brine. *Journal of Nuclear Materials*, **323**, 1–7.
Miyata, S. (1975) The synthesis of hydrotalcite-like compounds and their structures and physic-chemical properties. *Clays and Clay Minerals*, **31**, 369–375.
Miyata, S. (1980) Physicochemical properties of synthetic hydrotalcites in relation to composition. *Clays and Clay Minerals*, **28**, 50–56.
Miyata, S. and Kumura, T. (1973) Synthesis of new hydrotalcite-like compounds and their physicochemical properties. *Chemistry Letters*, 843–848.
Newville, M. (2001) IFEFFIT: Interactive XAFS analysis and FEFF fitting. *Journal of Synchrotron Radiation*, **8**, 322–324.
Prasanna, S.V., Kamath, P.V., and Shivakumara, C. (2007) Synthesis and characterization of layered double hydroxides (LDHs) with intercalated chromate ions. *Materials Research Bulletin*, **42**, 1028–1039.
Renaudin, G., Kubel, F., Rivera, J.P., and Francois, M. (1999) Structural phase transition and high temperature phase structure of Friedels salt, $3CaO{\cdot}Al_{j2}O_3{\cdot}CaCl_2{\cdot}10H_2O$. *Cement and Concrete Research*, **29**, 1937–1942.
Radha, A.V., Kamath, P.V., and Shivakumara, C. (2007) Order and disorder among the layered double hydroxides: combined Rietveld and DIFFaX approach. *Acta Crystallographica Section B: Structural Science*, **63** 243–250.
Rives, V. (2001) *Layered double hydroxides: Present and future*. Nova Science Publishers, New York.
Rozov, K., Berner, U., Taviot-Gueho, C., Leroux, F., Renaudin, G., Kulik, D., and Diamond, L.W. (2010) Synthesis and characterization of the LDH hydrotalcite-pyroaurite solid-solution series. *Cement and Concrete Research*, **40**, 1248–1254.
Rozov, K., Berner, U., Kulik, D., and Diamond, L.W. (2011) Solubility and thermodynamic properties of carbonate-bearing hydrotalcite-pyroaurite solid solutions with 3:1 Mg/(Al+Fe) mole ratio. *Clays and Clay Minerals*, **59**, 215–232.
Shannon, R.D. (1976) Revised effective ionic-radii and systematic studies of interatomic distances in halides and chalcogenides. *Acta Crystallographica Section A*, **32**, 751–767.
Shock, E.L., Sassani, D.C., Willis, M., and Sverjensky, D.A. (1997) Inorganic species in geologic fluids: Correlations among standard molal thermodynamic properties of aqueous ions and hydroxide complexes. *Geochimica et Cosmochimica Acta*, **61**, 907–950.
Taylor, R.M. (1984) The rapid formation of crystalline double hydroxy salts and other compounds by controlled hydrolysis, *Clay Minerals*, **19**, 591–603.
Thomas G.S., Rajamathi, M., and Kamath, P.V. (2004) Diffax simulations of polytypism and disorder in hydrotalcite. *Clays and Clay Minerals*, **52**, 693–699.
Treacy, M.M.J., Newsam, J.M., and Deem, M.W. (1991) A general recursion method for calculating diffracted intensities from crystals containing planar faults. *Proceedings of the Royal Society, A*, **433** 499–520.
Trolard, F., Bourrie, G., Abdelmoula, M., Refait, P., and Feder, F. (2007) Fougerite, a new mineral of the pyroaurite-iowaite group: Description and crystal structure. *Clays and Clay Minerals*, **55**, 323–334.
Ufer, K., Kleeberg, R., Bergmann, J., Curtius, H., and Dohrmann, R. (2008) Refining real structure parameters of disordered layer structures within the Rietveld method,

Zeitschrift für Kristallographie Supplements, **2008**, 151–158.

Unnikrishnan, R. and Narayanan, S. (1999) Metal containing layered double hydroxides as efficient catalyst precursors for the selective conversion of acetone. *Journal of Molecular Catalysis A: Chemical*, **144**, 173–179.

Weiss, A. and Toth, E. (1996) Untersuchungen zur Synthese, Quellungseigenschaften und Anionenaustausch von kristallchemisch modifizierten Doppelhydroxiden vom Hydrotalkit-Typ. *Jahrestagung der DTTG-Freiberg*, 267–276.

Wilke, M., Farges, F., Petit, P.E., Brown, G.E., and Martin, F. (2001) Oxidation state and coordination of Fe in minerals: An FeK-XANES spectroscopic study. *American Mineralogist*, **86**, 714–730.

(*Received 10 December 2012; revised 16 October 2013; Ms. 734; AE: A. Thompson*)